Brownian Motion of Inert Tracer Macromolecules in Polymerized and Spontaneously Bundled Mixtures of Actin and Filamin

Li Hou,* Katherine Luby-Phelps,‡ and Frederick Lanni§

Center for Fluorescence Research in Biomedical Sciences and Departments of *Physics, ‡Chemistry, and §Biological Sciences, Carnegie-Mellon University, Pittsburgh, Pennsylvania 15213

Abstract. By use of light microscopy and fluorescence photobleaching recovery, we have studied (*a*) structures that form in a system composed of copolymerized rabbit muscle actin and chicken gizzard filamin and (*b*) the Brownian motion of inert tracer macromolecules in this matrix. We have used as tracers size-fractionated fluorescein-labeled ficoll and submicron polystyrene latex particles. In F-actin solutions, the relative diffusion coefficient of the tracer was a decreasing function of both tracer size and actin concentration. Also, a percolation transition for latex particle mobility was found to follow a form suggested by Ogston (Ogston, A. G. 1958. *Trans. Faraday Soc.* 54:1754–1757) for random filament matrices. The inclusion of filamin before polymerization resulted in increased tracer mobility. Below a filamin dimer-to-actin monomer ratio of 1:140, no structural features were observed in the light microscope. At or above this ratio for all actin concentrations tested, a three-dimensional network of filament bundles was clearly discriminated. Latex particles were always excluded from the bundles. By use of a dialysis optical cell in which polymerization could be initiated with very little hydrodynamic stress, we found that filamin can spontaneously bundle F-actin. A simple physical picture explains how dynamics can affect the structural result of coassembly and provides a further hypothesis on the balance between random filament cross-linking and large-scale bundling. Control of this balance may be important in cytoplasmic motile events.

THE motile machinery of nonmuscle cells must be versatile enough to serve several different functions. The well-known actin stress fiber array that occurs in the cytoplasm of adherent tissue culture cells is disassembled and rearranged for ameboid locomotion and for cleavage during mitosis. There is considerable evidence from electron microscopy of fixed cells (Wolosewick and Porter, 1979; Schliwa and van Blerkom, 1981; Gershon et al., 1985) and, more recently, from optical microscopy of live cells (Jacobson and Wojcieszyn, 1984; Luby-Phelps et al., 1986, 1987, 1988; Luby-Phelps and Taylor, 1988) that the cytoplasmic ground substance has gel-like properties that nevertheless allow for internal transport of organelles, translocation of actin fibers (Heath, 1983; Fisher et al., 1988), and diffusion of macromolecules. To better understand the operation of the intracellular motile system, we have made simple reconstituted systems that show some of the properties observed in live cells or in isolated cytoplasm.

Here we have investigated the system composed of actin and filamin in an attempt to reconstitute a gel of interconnected actin filaments. It is known from electron microscopy and rheometry and from measurements of fluorescence photobleaching recovery (FPR)[1], and dynamic light scattering (Kawamura and Maruyama, 1970; Zaner and Stossel, 1983; Lanni and Ware, 1984; Janmey et al., 1986, 1988; Buxbaum et al., 1987; Simon et al., 1988*a*,*b*) that actin filaments reach an average length of many microns. Filamin is a bivalent, dimeric, actin-binding protein with a molecular mass of 500 kD and has a long, flexible, rod-like structure with a span of 160–193 nm (for review see Weihing, 1985). The interaction of actin and filamin has been measured mainly via rolling-ball viscometry, sedimentation, and electron microscopy (Wang and Singer, 1977; Hartwig and Stossel, 1979; Fechheimer et al., 1982; Rockwell et al., 1984). The principal result of these experiments has been the characterization of an actin–filamin gel-like phase. In the experiments reported here, we have used native proteins and have measured the diffusion rate of fluorescent inert macromolecules in the reconstituted, polymerized actin–filamin mixtures. The diffusion coefficient of inert, compact particles is of interest for two reasons. First, since ideal inert particles interact with the surrounding matrix only via hydrodynamic coupling and obstruction effects, their diffusion rate sets an upper limit on the mobility of proteins of comparable size that might also interact with the matrix via specific and nonspecific chemical and electrostatic binding or repulsive forces. Second, the dependence of the tracer diffusion coefficient on matrix concentration and on tracer size will reflect the structural features of the matrix and the degree of Brownian motion of

1. *Abbreviations used in this paper*: FPR, fluorescence photobleaching recovery; PSL, polystyrene latex; SEC, size exclusion chromatography.

the matrix elements. Since in most reconstituted biopolymer systems important structural features are below the resolution limit of the light microscope, measurements of tracer diffusion can be used to estimate structural parameters indirectly. Finally, it was of interest to us to determine whether a cross-linked filament network can be distinguished from an un-cross-linked suspension of long filaments by the form of the dependence of the inert particle tracer diffusion coefficient on tracer particle size.

It was our hypothesis that by cross-linking randomly oriented actin filaments into a gel network, diffusion of inert macromolecules in the matrix would be slowed. This effect would be more severe for particles comparable in size with the average mesh of the network and would result in immobilization of particles large enough to be trapped in finite voids of the network. Instead, we found that submicron particles could be immobilized (diffusion coefficient $<5 \times 10^{-11}$ cm^2/s) in solutions of F-actin alone, in partial agreement with previous observations by Tait and Frieden (1982). We also found, in contrast to our expectations, that inclusion of filamin in the polymerization mixture did not lower the tracer particle diffusion coefficient.

Materials and Methods

Reagents and Buffer Solutions

FITC isomer I, Tris, EGTA, EDTA, PMSF, and BSA were obtained from Sigma Chemical Co. (St. Louis, MO). Reagent-grade inorganic salts KCl, NaCl, $CaCl_2$, and $MgCl_2$ were from J. T. Baker Chemical Co. (Phillipsburg, NJ). DTT and ATP were from Boehringer Mannheim Biochemicals (Indianapolis, IN). Sodium azide (NaN_3) was from EM Science (Cherry Hill, NJ). Distilled deionized water was used in all buffer preparations.

Buffer compositions were as follows: (buffer A) 2 mM Tris, 0.2 mM $CaCl_2$, 0.2 mM ATP, 0.2 mM DTT, 0.01% NaN_3, pH 8.0, at 5°C; (polymerization buffer) buffer A with 100 mM KCl and 2 mM $MgCl_2$; (buffer D) 20 mM Tris, 1 mM EDTA, 1 mM EGTA, 0.2 mM DTT, 0.02% NaN_3, 0.2 mM PMSF, pH 8.0, at 0°C; (buffer H) buffer D with 300 mM NaCl; and (buffer S) 10 mM Tris, 50 mM KCl, 0.02% NaN_3, pH 8, at 20°C. All buffers for protein chromatography were used at 4°C.

Actin Preparation

Actin was extracted from an acetone powder of rabbit skeletal muscle according to the procedure of Spudich and Watt (1971). G-actin was freeze-dried in sucrose (2 mg/mg actin) and stored at −20°C. For use, 10–20 mg actin was dissolved in 2–5 ml buffer A and dialyzed overnight in 2 × 500 ml. The actin was then clarified by centrifugation at 2×10^5 *g* for 2 h at 4°C. The actin concentration in the supernatant was determined by absorbance difference (ΔA) at 290 and 340 nm. An extinction coefficient of 0.63 per milligram per milliliter (Houk and Ue, 1974) was used to convert ΔA to concentration. G-actin was stored on ice and used within 48 h.

Gel-filtered actin was prepared by size exclusion chromatography (SEC) in buffer A on a 2-cm-diameter × 40-cm column of Sephadex G-150 (Pharmacia Fine Chemicals, Piscataway, NJ). Trailing fractions from the second band in the protein absorbance chromatogram were pooled for use. Gel-filtered G-actin was stored on ice and used within 6 h.

The polymerization rate of actin used in these experiments was checked by measuring light scattering at an angle of 90° after addition of KCl to 100 mM and $MgCl_2$ to 2 mM. The characteristic lag phase preceding rapid polymerization (Kasai et al., 1962; Tobacman and Korn, 1983) was observed for both types of actin, typically 0.5–1 min for 0.6 mg/ml standard actin and 2–3 min for 0.6 mg/ml gel-filtered actin.

Filamin Preparation

Filamin was prepared from frozen chicken gizzards (Pel-Freeze Biologicals, Rogers AR) by following the procedure of Wang (1977) with some modifications based on our observation that filamin did not adsorb to hydroxylapatite, while many of the other extracted proteins did. After steps 1 and 2 of the published procedure, the supernatant was dialyzed in buffer D and adsorbed to a 2.5-cm-diameter × 30-cm column of DEAE-cellulose (DE-53; Whatman Inc., Clifton, NJ). The column was washed with 200 ml buffer D and eluted with a 500-ml 0–0.5 M NaCl linear gradient. The fractions containing filamin were identified by SDS-PAGE, pooled, and applied to a 4-cm-diameter × 20-cm column of fast-flow hydroxylapatite (No. 391974, lot 710011; Calbiochem-Behring Corp., La Jolla, CA) in buffer H. The flow-through fraction was dialyzed in buffer D and readsorbed on the DE-53 column. A 300 mM NaCl step elution was used to obtain a reconcentrated filamin fraction. SDS-PAGE showed that actin was a minor contaminant at this point. SEC on a 4-cm × 100-cm column of Sepharose CL-6B (Pharmacia Fine Chemicals) in buffer H was then used to separate filamin from contaminating actin. Purified filamin was then stored on ice in buffer H at a protein concentration >0.25 mg/ml. Filamin prepared and stored in this way retained its activity for >4 mo. The yield was typically 8 mg filamin from 30 g trimmed gizzards.

For use, filamin was dialyzed in buffer A and reconcentrated when necessary by vacuum dialysis in 2-ml collodion membrane bags (Schleicher & Schuell, Inc., Keene, NH). Filamin concentration was determined by absorbance difference at 280 and 340 nm, with an extinction coefficient of 0.66 per milligram per milliliter (Wang, 1977). Filamin activity was assayed by rolling-ball viscometry of serially diluted filamin stock copolymerized for 1 h with 0.6 mg/ml actin. Other copolymerized mixtures were tested the same way, following the general procedures of MacLean-Fletcher and Pollard (1980).

Fluorescent Ficoll Tracers

The preparation and use of these polymers has been recently discussed by Luby-Phelps (1989). Ficoll 400 (Pharmacia Fine Chemicals) was activated and labeled at low density with FITC by following the procedure of Inman (1975). The labeled polymer was fractionated by SEC on a 100-cm column of Sepharose CL-6B (Pharmacia Fine Chemicals) in buffer S. Fractions of 3.5 ml were collected and stored in small aliquots at 4°C for use or dialyzed in water, lyophilized, and stored at −20°C for extended use.

FPR (see below) was used to determine the molecular size of ficoll in fractions used in our experiments. FPR specimens were prepared containing dilute fluorescent ficoll in polymerization buffer. The diffusion coefficient (D_o) was calculated from the FPR data for each specimen, and the molecular hydrodynamic radius (R_H) was calculated from D_o by use of the Stokes–Einstein relation: $D_o = kT/6\pi\eta R_H$. Under optimal conditions, we could determine D_o with standard deviation of 1.7%, but we point out that D_o is itself an average over the dispersity in the ficoll sizes in each fraction. The effect of polydispersity is not severe in dilute solution but becomes significant when the size of the tracer molecules is close to the mesh of the surrounding matrix (Kathawalla and Anderson, 1988). In the experiments reported here, the largest ficoll tracer used was still significantly below the mesh of the most concentrated F-actin matrix.

Polystyrene Latices

Fluorescent polystyrene latex (PSL) microspheres were obtained as 10% suspensions (Polysciences, Inc., Warrington, PA) in the sizes (diameters) 0.05, 0.10, 0.23, 0.51, and 0.70 μm. FPR measurements (see below) showed these particles, as received, to have a high affinity for actin filaments (Fig. 1). Adsorption of BSA to the latex particles eliminated this problem. To prepare BSA-coated PSL, the suspensions were first dialyzed in distilled water. 70 μl of each suspension was then mixed with 1 ml of 2% BSA in buffer A and stored on ice until use. For some experiments, we removed excess BSA from the latices by use of 0.22- or 0.025-μm filter membranes (types GSWP and VS; Millipore Continental Water Systems, Milford, MA).

FPR

Instrumentation and data analysis followed Simon et al. (1988*b*). A beam expander and plano-convex lens were used to bring a laser beam through the fluorescence excitation optics to a focus at the microscope specimen plane. The gaussian beam diameter ($2w_o$) was determined by scanning the image of the beam on a fluorescent thin film and was typically 55 μm with a 6.3× objective lens and 20 μm with a 16× objective lens. The algorithm of Yguerabide et al. (1982) was used for analysis of fluorescence recovery data, giving the recovery time constant ($t_{1/2}$), the diffusion coefficient (D), and mobile fraction (percent recovery; %Rec) of the tracer. In general, data record duration exceeded the recovery time constant by at least a factor of 10.

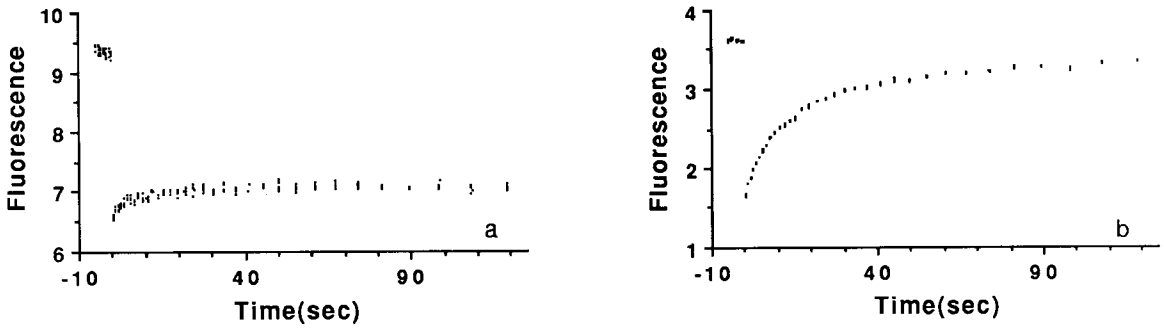

Figure 1. FPR data for 0.10 μm PSL particles in 1 mg/ml F-actin. *a* is of untreated PSL particles in polymerized actin and shows an incomplete fluorescence recovery of 7%. *b* is of BSA-treated PSL in an otherwise identical specimen and shows 100% recovery. The recovery time constant is approximately the same in the two cases. Abscissa is elapsed time (in seconds), and ordinate is linear in fluorescence detector photocurrent. The relatively low signal-to-noise ratio of these data is due mainly to number fluctuations resulting from the low number density of PSL particles in the specimen. 1 mg/ml actin is far below the percolation cutoff concentration (>8 mg/ml) for this PSL (see Table II).

Microscopy

Video-enhanced contrast images were recorded in differential interference contrast (DIC), polarization, and phase-contrast modes by use of a newvicon camera (NC65SX; Dage-MTI Inc., Michigan City, IN) or a chalnicon camera (01-HD; Hamamatsu Photonics, Chicago, IL), and an image processor (C1966; Hamamatsu Photonics). Images were recorded on videotape for later playback, averaging, and photography. DIC, polarization, and phase-contrast optical systems (Carl Zeiss, Inc., Thornwood, NY) were used with a 100× 1.25-NA plan-achromat lens or a 63× 1.25-NA plan-neofluar phase-contrast lens.

As an alternative method to estimate the diffusion coefficient (D_e) of PSL particles in F-actin specimens, the two-dimensional displacement (r_i) of individual PSL particles in a video field was measured at a minimum of six time intervals (t_i), ranging from 10 to 160 s. The estimate was computed as $D_e = \text{avg}[(r_i)^2/4t_i]$.

Specimen Preparation

Flat drawn borosilicate glass capillary tubes with inner dimensions 0.1 mm deep × 0.8 mm wide × 50 mm (No. 5010; Vitro Dynamics Inc., Rockaway, NJ) were used for all FPR and microscopy experiments except as noted. Since occasional batches of these tubes showed strong binding affinity for ficoll and proteins, all capillary tubes were treated by washing with 2% BSA, rinsing with water, and drying by air flow. FPR specimens were prepared by mixing at 5°C G-actin, filamin, and tracer particles, all in buffer A, to a total volume of 50 μl in a 0.5-ml plastic tube. Polymerization was initiated by adding KCl to 100 mM and $MgCl_2$ to 2 mM using a small volume of a concentrated stock solution. The specimen was quickly mixed on a mechanical vortexer and drawn into a capillary tube. The tube was sealed at the ends with liquid plastic to a flat black-anodized aluminum plate for FPR or to a glass slide for microscopy. Specimens were allowed to stand overnight at room temperature in the dark before testing.

Systematic errors in determination of protein concentration and in FPR laser beam diameter measurement were the most significant sources of variation in our experiments. Since a complete set of FPR measurements required up to 9 h of instrument time, our best results were obtained by preparing all specimens from fresh stock solutions and making all FPR records in one operating session on the next day. No systematic differences were found as a function of specimen aging in this time period.

Specimen composition varied over the 0–5-mg/ml actin range, a 0–0.03 molar ratio of filamin dimer (500 kD) to actin (42 kD), and the 8–700-nm-diameter size range of various ficoll or PSL tracers. Tracer concentration was always very low; i.e., the tracer volume fraction was always much less than 1.00. For PSL-containing microscopy specimens, 1 μl of 0.7% PSL was added to 49 μl of protein solution, giving a final tracer volume fraction of 10^{-4}. Ficoll volume fractions were comparable. For dialysis optical cell specimens, the PSL volume fraction was 1.4×10^{-5}. For comparison purposes, actin volume fraction at 1 mg/ml is $\sim 3 \times 10^{-3}$.

Nine ficoll fractions selected to span the SEC chromatogram of Ficoll 400 were used in the preparation of F-actin and filamin-actin specimens and of reference specimens containing no protein. A minimum of eight FPR records were analyzed for each specimen, and the average diffusion coefficient and fractional recovery were calculated. For the ficoll in each reference specimen, the diffusion coefficient (D_0) was used to calculate an average hydrodynamic radius ($\langle R_H \rangle$), which ranged from 4.4 to 29 nm (Table I). For each specimen containing F-actin (1, 3, and 5 mg/ml), the diffusion coefficient of the ficoll tracer (D) was divided by the corresponding reference value (D_0) to give the relative diffusion coefficient. D/D_0 was computed in the same way for ficolls in filamin-actin specimens.

F-actin FPR specimens were also prepared in the range of 0–9 mg/ml for each of the five PSL tracers used. For each size PSL, the filament density at which there was a percolation cutoff was estimated by finding the lowest concentration of F-actin for which fluorescence recovery of the PSL did not occur. This clearly defines the cutoff in terms of the size of the FPR pattern in the specimen; i.e., for an actin concentration above each cutoff, PSL particle diffusion could only occur over a range much smaller than 20 μm.

Dialysis Optical Cell

This device was designed so that actin could be homogeneously polymerized with no convective mixing during high-resolution microscopical observation (Fig. 2). In use, the assembled cell was first flushed extensively with buffer A. The specimen was then loaded into the upper cell half, and the upper valves were closed. The dialysis cell was then mounted on the microscope and perfused through the lower cell half. Salts such as KCl and $MgCl_2$ have diffusion coefficients in the range of $1–2 \times 10^{-5}$ cm^2/s at 25°C and therefore equilibrate across the specimen in 20–40 s, limited by the permeability of the dialysis membrane. As long as the pressure drop across the cell during perfusion was limited, steady-state deformation of the dialysis membrane was small. An overall pressure drop of 36 cm was used, with the microscope stage at 18 cm. A tuberculin needle (Becton-Dickinson & Co., Rutherford, NJ) was used as a ballast at the drain end and immersed in a few millimeters of water to prevent dripping which caused flow and focus transients at the microscope. The perfusion flow rate was always close to 0.5 ml/min with this setup. To eliminate flow transients in the specimen due to opening or closing valves, perfusion was run throughout the observation period. Switching to polymerization buffer caused a flow transient, but the inlet tubing volume provided a 26-s period for this to damp out before polymerization buffer reached the optical cell.

Table I. Diffusion Data for Ficoll Fractions in Buffer

Fraction	D_0	$\Delta D/D_0$	$\langle R_H \rangle$	$\langle \%Rec \rangle$
No.	$\mu m^2/s$		*nm*	*%*
91	8.0	0.05	29.0	100.0
101	10.3	0.02	22.6	99.3
111	13.0	0.03	17.9	99.2
121	15.9	0.02	14.6	101.0
131	20.8	0.04	11.2	100.4
141	27.6	0.03	8.5	100.5
151	36.2	0.03	6.4	100.2
161	42.9	0.03	5.4	100.7
171	53.1	0.03	4.4	100.2

$\Delta D/D_0$ is the root mean square fractional error in D_0.

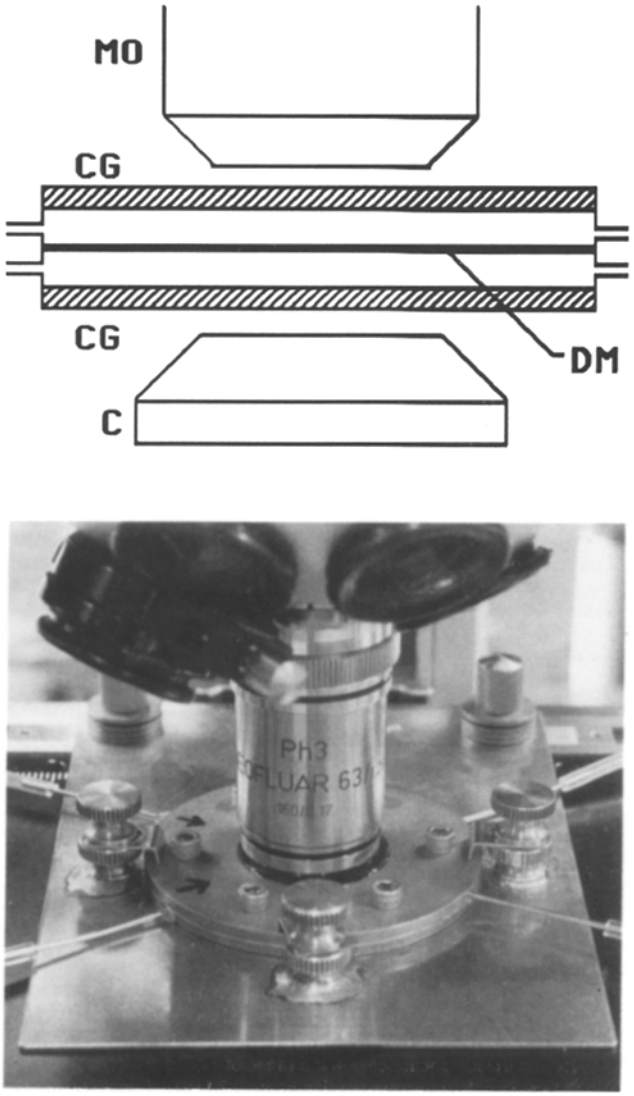

Figure 2. Dialysis optical cell. Upper and lower cell halves were machined from 5-cm disks of stainless steel and were identical except for a hexagonal array of clear screw holes in the upper piece that matched to 8–32 threaded holes in the lower. A 25-mm round cover glass window was cemented in each cell half, forming matching shallow wells 0.285 mm deep and 144 μl in volume. The cell was assembled with a sheet of 0.043-mm hydrated dialysis membrane (SpectraPor 2, 45 mm flat width, 12 kD MWCO; Spectrum Medical Industries, Los Angeles, CA) sandwiched between the cell halves. Shallow channels milled in each disk were connected to 1-mm stainless steel tubing, and formed diametrically opposed inlet and outlet passages for filling the upper cell half and perfusing via the lower. The overall window-to-window thickness of the dialysis cell was 0.95 mm, slightly less than a standard microscope slide, so that oil-immersed condenser and objective lenses could be adjusted for Koehler illumination. Schematic (not to scale) shows cover glass windows (*CG*), dialysis membrane (*DM*), and microscope objective (*MO*) and condenser (*C*) lenses. Photograph shows assembled cell mounted on microscope with inlet and outlet tubing for specimen compartment and for perfusion.

The dialysis membrane used in these experiments was found to be birefringent. This, and the moderate light scattering cross section of the membrane, reduced the contrast of the DIC image. Rotation of the membrane so that one principal axis coincided with the shear axis of the DIC optics minimized but did not eliminate this effect. The phase-contrast image was not severely affected, and the fluorescence image was unaffected.

Results

Mobility of Tracer Ficolls in F-Actin Solutions and in Filamin–Actin Mixtures

In specimens containing 1, 3, and 5 mg/ml F-actin, D/D_o was found to be a decreasing function of both actin filament concentration and the size of the ficoll macromolecules (Fig. 3). Complete fluorescence recovery was always observed, even for the largest ficoll tracer (R_H = 29 nm) in 5 mg/ml actin. In a separate experiment, we compared gel-filtered with standard actin in matched FPR specimens containing 1.4 mg/ml actin and tracer ficolls of three sizes: R_H = 4.5, 13, and 34 nm. No differences in D or *%Rec* were found within experimental error.

Addition of filamin in molar ratio to G-actin of 1:270, 1:140, 1:70, and 1:35 before polymerization did not result in lower tracer ficoll diffusion coefficients as determined by FPR. In general, D decreased with actin concentration as expected but increased weakly with filamin-to-actin ratio (F:A); the increase was proportionally greater for larger ficolls (Fig. 3). In all specimens, the fluorescence recovery was ≥97%.

Optical Microscopy of Capillary Tube Specimens

The result of copolymerizing filamin with actin was found to be a simple function of F:A. DIC and phase-contrast images of F-actin solutions (F:A = 0) in the range of 0.5–5 mg/ml showed no features above background. This was also the case for specimens containing filamin at molar ratios ≤1:210. At F:A ≥1:140, a three-dimensional network of randomly oriented, interconnected fibers was clearly visible. The critical ratio relationship for this structural transition is clearly shown by a pseudo-phase diagram representation of all copolymerized mixtures tested (Fig. 4). Scans of centimeter-long tracts, as well as axial scans from the cover glass to the working distance of the objective lens (~100 μm), showed the same network structure throughout the specimen. Gel-filtered actin was also tested and showed the same transition for 1:210 < F:A < 1:140 as all other specimens.

Several physical properties of the fiber network were inferred from optical images (Fig. 5). The number density of fiber segments increased with actin concentration but showed no strong dependence on filamin concentration as long as F:A was ≥1:140. The contrast of individual fibers increased with F:A, indicating higher protein content within each fiber. Brownian motion of the network strands was undetectable at the resolution limit (0.2 μm), suggesting a considerable rigidity to the strands and a high degree of interconnection. Fiber diameters were estimated from the DIC image to be ~1 μm. The average void region diameter was ~10 μm at 0.5 mg/ml and noticeably less at 1 mg/ml. Polarization micrographs showed that the fiber strands oriented approximately in the focal plane were birefringent. Occasional strands were of large enough diameter to be seen to be intrinsically birefringent, showing that the fibers were most probably bundles of parallel actin filaments cross-linked by filamin molecules, the intrinsic birefringence of the fibers in this case being due to the form birefringence of the parallel filaments.

Two properties of the structural transition were defined by observation of the Brownian motion of BSA-treated PSL particles included in the copolymerization mixture. In specimens forming a fiber network, the particles were never found

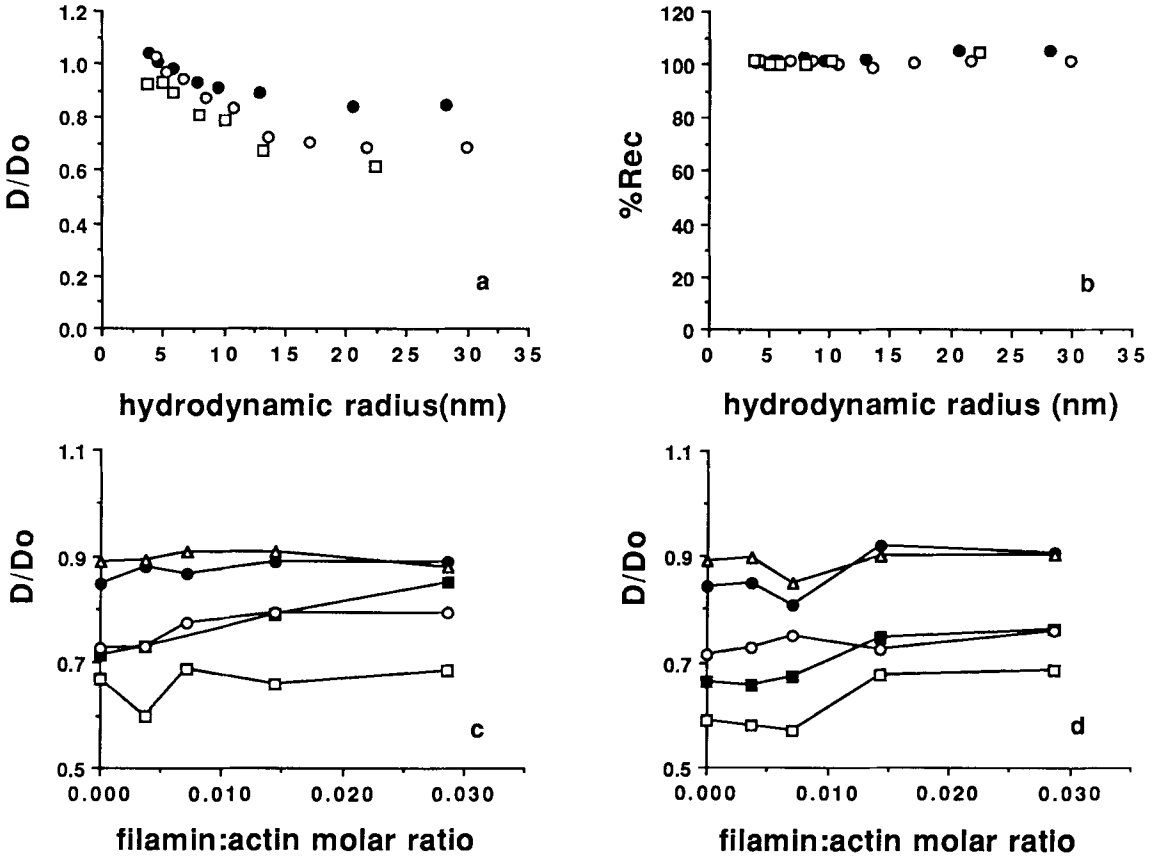

Figure 3. Diffusion of ficoll tracers in F-actin and filamin-actin matrices. As a function of tracer hydrodynamic radius, F-actin reduces the tracer diffusion coefficient (*a*) but does not reduce the mobile fraction in the range tested (*b*). In *a* and *b*: (●) 1; (○) 3; and (□) 5 mg/ml actin. As a function of filamin-to-actin molar ratio, D/D_o increased weakly for most ficoll fractions tested in 3 (*c*) and 5 mg/ml actin (*d*). All tracers were 100% mobile as in *b*, and the same results were obtained in 1 mg/ml actin. In *c* and *d*, symbols refer to ficoll fractions (see Table I): (△) No. 171; (●) No. 141; (○) No. 121; (■) No. 101; and (□) No. 91, where lower numbers correspond to larger ficoll molecules.

attached to or incorporated within the bundles but were always mobile in the void spaces. Secondly, Brownian motion of the PSL particles was increased in bundled specimens relative to the corresponding F-actin specimen (Fig. 6). Above the critical *F:A* ratio, the degree of Brownian motion increased with *F:A*.

Rolling-ball viscometry results on the same mixtures used for microscopy were similar to those of Rockwell et al. (1984), showing no sharp transition but rather a steep monotonic increase in apparent viscosity with *F:A*.

Percolation Cutoff in F-Actin Solutions

Over the actin concentration range of 0–9 mg/ml, we found by FPR sequentially higher percolation cutoffs for the three largest PSL tracers used. The actin concentration ranges in Table II show the transition from slowed but relatively complete mobility to essentially complete immobility. For 0.51-μm particles, the Stokes–Einstein diffusion coefficient is 9×10^{-9} cm^2/s. By video microscopy, D_e was 2×10^{-9} cm^2/s in 0.55 mg/ml F-actin, and, in 0.65 mg/ml F-actin, D_e had dropped to 8×10^{-11} cm^2/s, a 25-fold decrease with only an 18% increase in filament density. In 0.70 mg/ml F-actin, only local Brownian motion of the PSL particles was detectable, with the average amplitude being less than the particle diameter. Approximately, an inverse square root relation was found between the filament concentration (c_{fil}) and the PSL particle size at the percolation cutoff (R_p); R_p = (constant) $\times$ $(c_{fil})^{-1/2}$.

Time Course of Copolymerization

Convection-free copolymerization processes were initiated and observed in the dialysis optical cell. No network structures were detected in pure actin specimens, but the retardation or immobilization of PSL particles as a result of actin polymerization was readily observed. When filamin and actin were copolymerized, formation of the three-dimensional bundle network could be observed by DIC or phase-contrast microscopy (Fig. 7). In phase contrast, small streak-like fibers appeared, bright or dark relative to background depending on axial displacement from the focal plane, with apparent random orientation. At first the fibers were undergoing considerable local motion, due both to Brownian processes and contractile deformations resulting from the binding interaction of actin and filamin. Over a period of seconds, these structures became longer and of greater contrast while undergoing motion of reduced amplitude. By the time the fibers were clearly interconnected, the motion of the network was almost undetectable. The image was static after ~3 min.

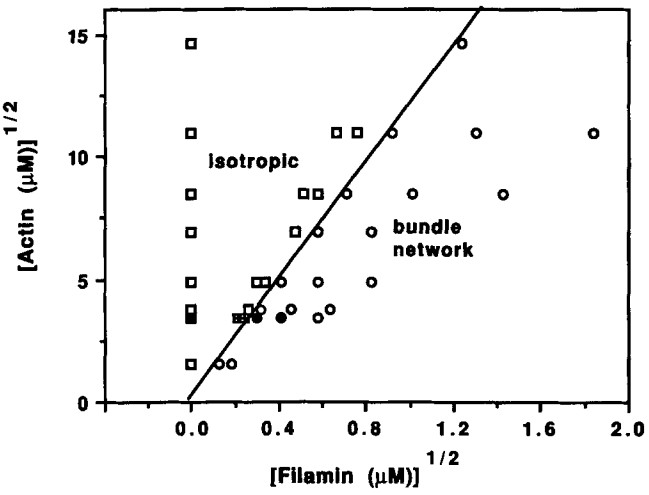

Figure 4. Structural transition in filamin–actin system. A phase diagram representation is used with the caution that the copolymerized structure is most likely a kinetically limited aggregate rather than at thermodynamic equilibrium. Axes are linear in the square root of protein concentration so that the large data range could be compactly represented. Symbols refer to filamin–actin mixtures tested: (○) bundle network observed by light microscopy; and (□) featureless matrix observed by light microscopy. Solid symbols are for gel-filtered actin specimens, and crossed symbols are mixtures for which both gel-filtered and standard actin were tested. The diagonal line is the locus for which *F:A* is ~1:140.

Discussion

Structural Features of the Filamin–Actin System

We initiated these experiments in an attempt to prepare isotropic gels of random actin filaments cross-linked by filamin that would otherwise have filament orientational distributions and spacings similar to F-actin solutions or similar to reconstituted gels containing actin and macrophage actin-binding protein (Hartwig and Stossel, 1979; Niederman et al., 1983). Such a gel would be a simple model for bulk cytoplasm. We have demonstrated instead that in the range of 0.5–5 mg/ml actin there is a structural transition in the copolymerized filamin–actin system. When filamin dimers are ≥ a 1:140 ratio to actin monomers, the copolymerization process results in formation of a large-scale, three-dimensional network of filament bundles. At or below 1:210, featureless, homogeneous matrices are observed at the resolution and contrast limits of the light microscope. Since diffraction-limited detection of filamentous structures having low linear mass density, such as acrosomal actin bundles and single microtubules, has been clearly demonstrated by video-enhanced contrast methods (Inoue, 1981; Schnapp, 1986; Cassimeris et al., 1988), any undetected filament alignment in our homogeneous filamin–actin matrices must be very tenuous. By use of the dialysis optical cell, we have shown the large-scale bundling to be spontaneous, in that it is driven by Brownian motion in the specimen and the binding potentials of the two proteins involved but requires no prior ordering of filaments such as would be caused by convective mixing.

There have been previous reports of gel and bundle formation in mixtures of actin with filamin-like proteins (Wang and Singer, 1977; Hartwig and Stossel, 1979; Rosenberg et al., 1981; Weihing, 1983; Rockwell et al., 1984). In general, gelation was assessed by viscometry or sedimentation, while bundles were detected by electron microscopy. Observations in two of these studies can now be understood as reflecting the structural transition. Hartwig and Stossel (1979) used cytochalasin B to reduce actin filament length, thereby increasing the concentration of filamin required to form sedimentable filament aggregates. Inspection of their Fig. 9 shows that the sedimentation-inhibiting effect of cytochalasin B vanishes at *F:A* approximately equal to 1:200. Notably, macrophage actin-binding protein was not equivalent to filamin in this assay. Most closely related to our work, Rockwell et al. (1984) found a sharp increase in the sedimentability of filamin–F-actin mixtures at a critical ratio in the range of 1:150 to 1:200.

The networks produced in our experiments can be compared with the actin-based gels originally isolated by Kane (1975, 1976) in sea urchin egg extracts. The extract gel bundles are needle-like, with angular interconnection and nearly paracrystalline order. They contain mainly actin, fascin (Otto et al., 1979), and small amounts of a spectrin-like protein (Mabuchi and Kane, 1987). Our filamin–actin bundles are curvilinear and show smooth interconnection. As discussed by Hartwig and Stossel (1981), Stossel et al. (1981), and Craig and Pollard (1982), long, flexible cross-linkers should allow for actin gelation without bundling. Therefore, it is significant that even without a compact cross-linker like fascin, filament bundles form readily in the filamin–actin system.

Our observation that both homogenous and bundled matrices can be assembled from filamin and actin show that factors in addition to macromolecular structure must be important in determining the result of assembly. When cross-linker is present during polymerization, assembly dynamics will also affect the final structure. If two singly cross-linked filaments are not entangled with other filaments on a scale comparable with their persistence length, Brownian motion will allow the linked segments to become more closely aligned and increase the probability of further cross-link formation. This cooperative process, when continued, will give rise to bundles until bundle stiffness and interconnection result in a structure that is too rigid to evolve further or until the cross-linker supply is exhausted. Cooperativity in filament alignment and cross-link formation is supported by our observation that PSL particles were never seen embedded in the network bundles. It is unlikely that this is due to a phase separation process because of the low PSL volume fraction and because the same network forms in the absence of PSL particles. A zippering process between aligning filaments would be effective in excluding compact particles.

The above model should hold for conditions where filaments are short or sparse and therefore not entangled, such as in the early stages of copolymerization. In support of this interpretation, we note that the highly ordered bundles observed by Kane (1976) form in a system that is limited by a very slow actin assembly rate. If filamin could be added to an F-actin solution without disturbing filaments (which is practically difficult since mixing causes tremendous shearing flow), we would predict that an isotropic actin network would result since the high degree of entanglement would drastically slow the rate at which filaments could align dur-

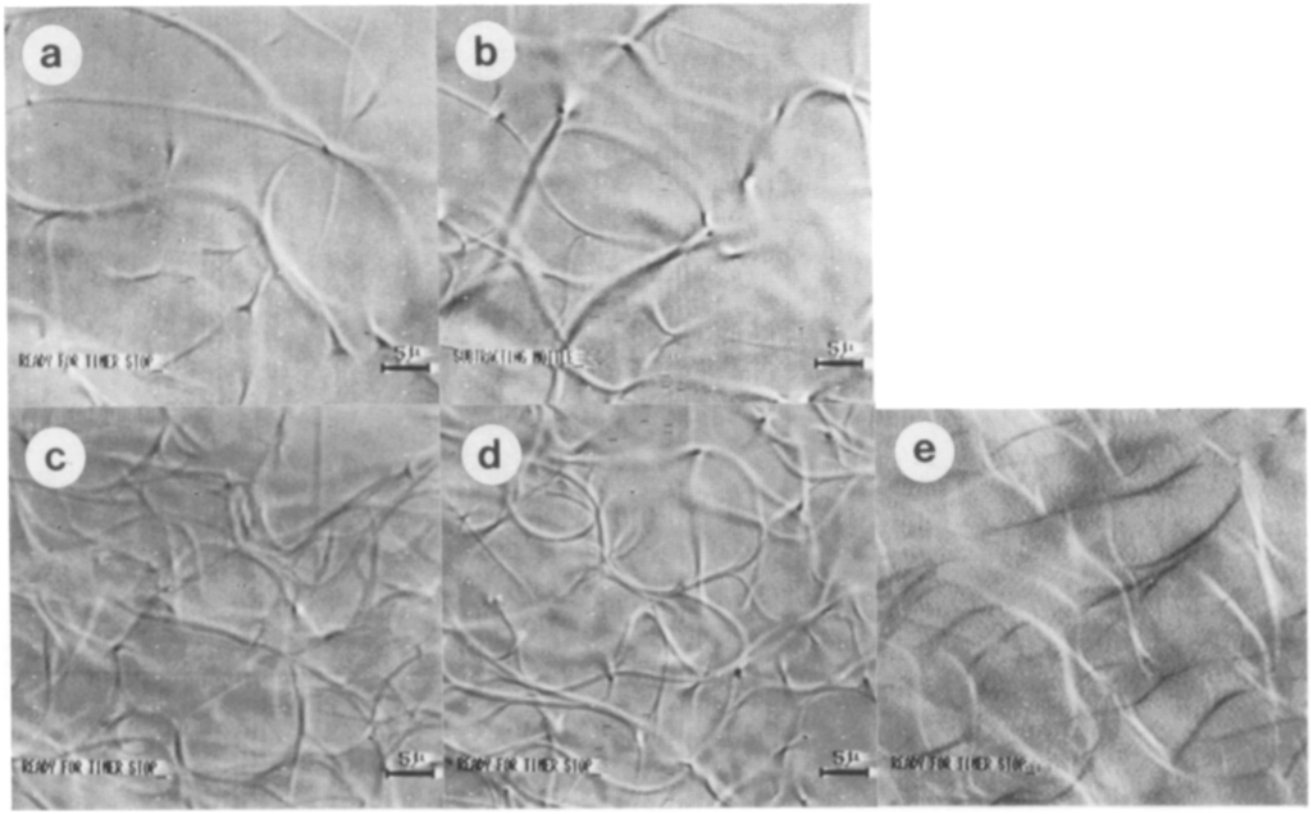

Figure 5. DIC and polarization microscopy of copolymerized filamin–actin mixtures having *F:A* >1:140. In *a* and *b*, actin concentration is 0.5 mg/ml, and *F:A* increases from 1:70 (*a*) to 1:35 (*b*). In *c* and *d*, actin concentration is 1 mg/ml, and *F:A* is 1:70 (*c*) or 1:35 (*d*). Horizontal comparison of the images shows that strand contrast increases with *F:A*. Vertical comparison shows that strand length density increases with actin concentration. In these micrographs the high-contrast dot-like features are network strands that are oriented axially rather than in the focal plane and can be followed through serial focal plane images. In specimens containing only actin, or with *F:A*<1:140, only featureless images were seen. Background images were obtained by averaging a transverse scan of the specimen at constant focal plane position. Displayed images were background subtracted and summed for 30 frames (1 s) for photography of still video images. Differential shear axis orientation is lower left to upper right at 45°. A polarization image (*e*) of a specimen identical to *d* shows the network strands to be highly birefringent. Polarizer orientation is parallel to sides of micrograph, analyzer is crossed. Bars, 5 μm.

ing cooperative cross-linking. This would be equivalent to copolymerization under conditions where the actin assembly rate was far greater than the cross-linking rate.

In this study, we have not observed gelation directly, but rather the bundling transition of actin filaments and the diffusion of tracers in each test matrix. The Flory model of multifunctional polymerization (Flory, 1953; Hartwig and Stossel, 1979) predicts that with constant weight average actin filament length the concentration of cross-linkers required to cause gelation should be proportional to the filament concentration. Since the normalized length distribution of F-actin well above its critical concentration is not a strong function of total actin (Oosawa, 1970; Kawamura and Maruyama, 1970), an approximate critical ratio relationship should be expected for gelation of the filamin–actin system. The Flory theory, however, was derived for covalently reacting systems in which it was realistic to assign equal reactivities to monomer and cross-linker molecules. This is generally not the case in biopolymer systems where the cross-linker interacts noncovalently with binding sites on an assembled filament. The degree of reaction for the monomer (G-actin) can be very different than the degree of reaction for the cross-linker (filamin) during the copolymerization process, giving rise to polymerization rate–dependent effects on structure. By the current study, we cannot resolve the question of whether the true gel point for the filamin–actin system occurs at the structural transition or at lower values of *F:A*. It is clear that at or above the transition assembly leads to a rigid gel network of filament bundles.

Transport in Filamin–Actin Matrices

In F-actin specimens, D/D_o for ficolls was found to be a weak, decreasing function of tracer size when compared with the intracellular measurements reported by Luby-Phelps et al. (1987). For ficolls in cytoplasm, D/D_o is significantly less than in 5 mg/ml F-actin, and the decrease with R_H is steeper and nearly linear. The data for cytoplasm may reflect the combined effects of a moderately concentrated protein solution containing entangled filaments. The separate contributions of filaments and globular macromolecules to the overall reduction in D/D_o for ficoll tracers in actin-based model systems is reported elsewhere (Hou, L., F. Lanni, and K. Luby-Phelps, manuscript submitted for publication).

Formation of cross-links or bundling caused by filamin within an F-actin matrix up to 5 mg/ml had no strong effects

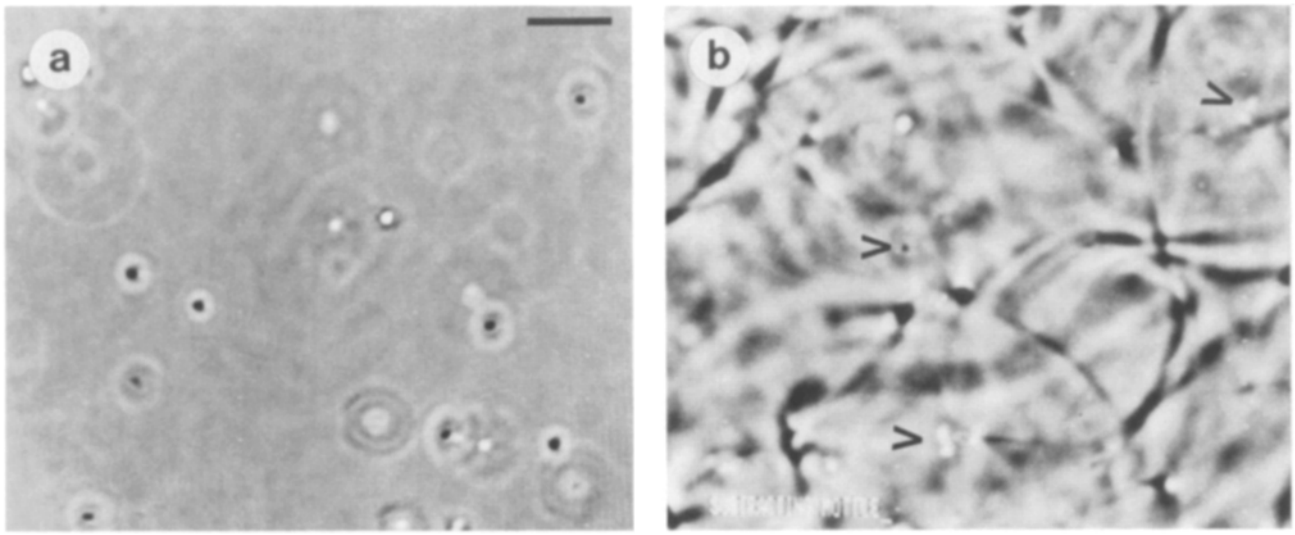

Figure 6. PSL microspheres show increased rate of Brownian motion at higher filamin-to-actin ratio. Phase-contrast images of 0.51 μm PSL particles in copolymerized filamin–actin mixtures were recorded as 30-frame (1 s) averages to show degree of PSL motion. In 1 mg/ml F-actin, 0.51 μm PSL shows no long-range mobility, and the corresponding image (*a*) shows sharply defined PSL particles. In *a*, the dark dot-like objects are in-focus particles, and the bright objects are PSL particles above or below the focal plane within a few microns. In *b*, *F:A* = 1:70, and PSL motion becomes more apparent over 1 s. Arrowheads mark images of single particles blurred by Brownian motion. At *F:A* = 1:35 (not shown), no particles were detectable in 1-s averages due to blurring by more rapid Brownian motion. In these specimens, the actin concentration and number density of PSL particles was the same. The filamin–actin network, in contrast, shows no detectable Brownian motion at this resolution. PSL motion in specimen *b* and at higher *F:A* ratio continued indefinitely. Bar, 10 μm.

on the diffusion of tracer ficoll molecules up to 29 nm in hydrodynamic radius (Fig. 3). We explain this as the net result of two opposing effects. Clustering or bundling of filaments increases the void volume accessible to a spherical tracer particle, allowing for freer diffusion in a large volume fraction of the system. At the same time, cross-linking makes parts of the existing network more compact, presenting a greater resistance to particles diffusing in dense regions of the system. The first effect is most important for particles comparable in size with the percolation cutoff of the filament matrix, and the second effect most important for small particles. If the ficoll tracers permeate the bundled regions to a significant degree, FPR would give an average diffusion coefficient that is only weakly a function of *F:A*, as observed. PSL particles, which are much larger and do not permeate the bundles, show a much larger diffusion rate increase with increasing *F:A*.

Table II. Percolation Cutoff Ranges for Polystyrene Latex Microsphere Diffusion in F-Actin

PSL particle diameter	F-actin cutoff concentration	$R_p\lambda_p^{1/2}$
μm	mg/ml	
0.70	0.40–0.45	1.42
0.51	0.65–0.70	1.31
0.23	3.7–4.0	1.41
0.10	>8	–
0.05	>8	–

At the highest actin concentration in each range shown, PSL particles were 100% immobile (see Results). $R_p\lambda_p^{1/2}$ is the product of the PSL particle radius (in microns) and the square root of the actin filament concentration (micron filament per cubic micron) at the percolation cutoff. In a system composed of randomly arranged long filaments, any property that depends on R should scale as the above product (Ogston, 1958). 1 mg/ml F-actin corresponds to λ = 39 μm filament/μm³.

Our observed percolation cutoffs for long-range diffusion of PSL in F-actin solutions (Table II) follow the form of the model derived by Ogston (1958). In the case of long filamentous obstructions, the void space distribution for spherical test objects is $p(R) = 2\pi LR \exp(-\pi LR^2)$, where R is the test object radius (in microns, for example), and L is the filament density in units of micron (filament) per cubic micron. $p(R)$ is the probability density that, given a random location in the void space of the system, a test sphere centered at that point could be expanded to radius R before the first contact is made with a filament. For this distribution, the most probable void radius (R_{MP}) is defined by $R_{MP}L^{1/2} = 0.4$, and the average void radius (R_{AV}) by $R_{AV}L^{1/2} = 0.5$. From our percolation data for 0.23-, 0.51-, and 0.70-μm-diameter PSL particles, we find an approximate relation for the percolation cutoff radius (R_P) to be $R_PL^{1/2} = 1.4$ (Table II). The existence of a percolation cutoff implies highly restricted Brownian motion of the actin filaments, the cause of the restriction being a topic of some debate (Tait and Frieden, 1982; Lanni and Ware, 1984; Zaner and Stossel, 1983; Simon et al., 1988*b*; Janmey et al., 1986, 1988). Certainly obstruction (entanglement) plays a major role, but the filament–filament binding potential has not been fully investigated.

Interpretation of our data rests on the assumption that ficoll and PSL tracers are inert, interacting with the matrix only via obstruction and hydrodynamic effects. Fluorescent ficolls were all 100% mobile in these experiments. The lowest ficoll diffusion coefficient measured was for the largest R_H fraction in 5 mg/ml F-actin, 4.8×10^{-8}cm²/s. In comparison, for a 10-μm actin filament diffusing without entanglements, a diffusion coefficient close to 3×10^{-9}cm²/s would be expected (Lanni and Ware, 1984). Measurements

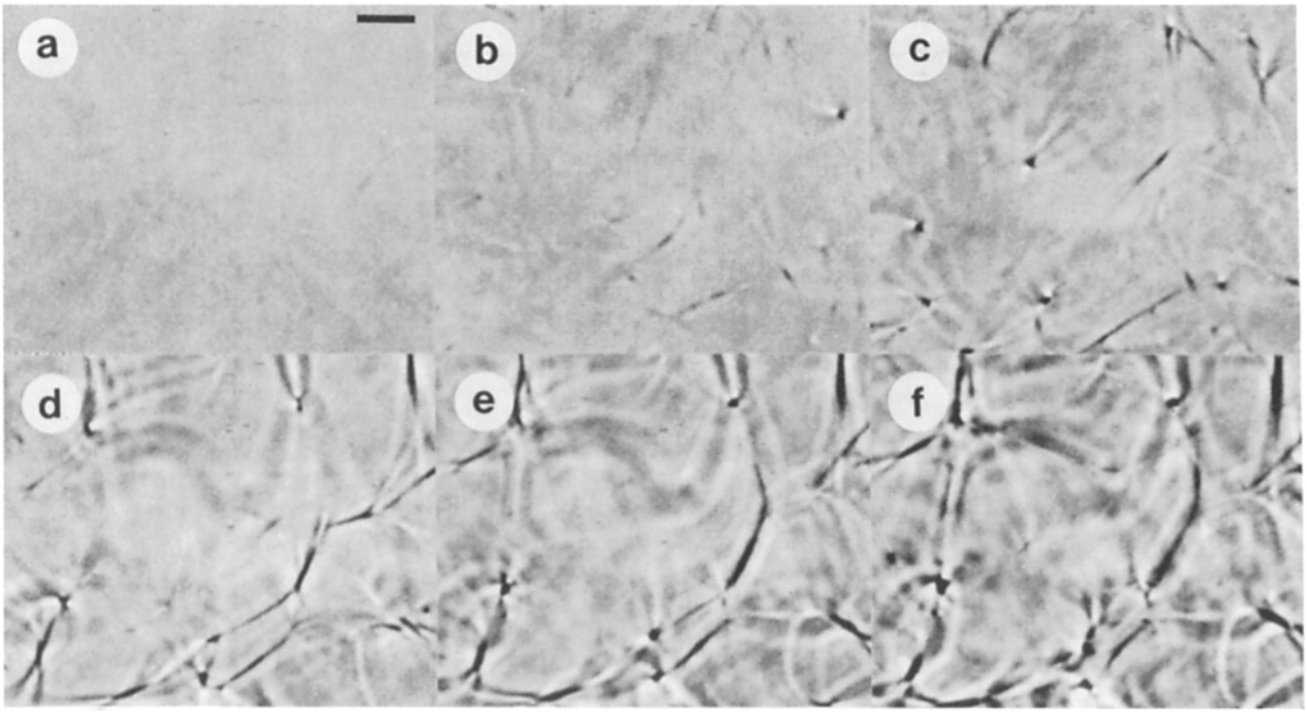

Figure 7. Time series showing actin filament bundle formation during copolymerization of filamin with 1 mg/ml actin and $F:A$ = 1:35. Phase-contrast micrographs show the spontaneous appearance of a three-dimensional network in the dialysis optical cell under zero-applied-shear conditions. Dialysis of the initial filamin–actin mixture against polymerization buffer was begun ~92 s before image *a*, in which the first traces of inhomogeneity were observed, was recorded. The subsequent images were at 112 (*b*), 132 (*c*), 152 (*d*), 172 (*e*), and 212 s (*f*). At early time points, the growing bundles appear to be in local Brownian motion which becomes highly restricted within 3 min. Displayed images were background subtracted as in Fig. 5 and summed for four frames (133 ms) for photography. Bar, 10 μm.

of F-actin diffusion coefficients have generally been below this estimate. It is clear that there cannot be any significant binding interactions between ficoll tracers and F-actin, otherwise the tracer would diffuse as slowly as the filament. PSL particles were found to have a binding affinity for F-actin, which was eliminated by adding BSA to the PSL suspension. This observation is in contrast to the quasi-elastic light scattering results of Newman et al. (1989) but may reflect the fact that long-range diffusion is measured by FPR, while a much smaller distance scale is usually monitored in quasi-elastic light scattering.

Summary

The fact that both homogenous and bundled matrices can be produced in the filamin–actin system at the light microscopic level indicates that factors in addition to intrinsic molecular properties can affect the result of supramolecular assembly. From a consideration of the physical forces acting in the system, we conclude that a more detailed model must include the rates of actin polymerization and cross-linking. The polymerization rate is itself a function of the nucleation rate and the elongation rate. An outstanding question is whether or not the gel point coincides with the structural transition generally. These factors are testable by the methods used here and by methods previously applied in the study of polymer gels.

We thank Judy Montibeller, Chrisanthe Thompson, and Ray Griffith for technical assistance; D. Lansing Taylor for critical review of this project at several stages; and William P. George for construction of the dialysis optical cell. We also thank the reviewers for many helpful comments and the editor for patience and encouragement.

This research was supported by grant GM34639 from the National Institutes of Health, DCB8616089 from the National Science Foundation, and AR32461 from the National Institutes of Health (to D. L. Taylor).

Received for publication 24 July 1989 and in revised form 10 January 1990.

References

Buxbaum, R.E., T. Dennerll, S. Weiss, and S. R. Heidemann. 1987. F-actin and microtubule suspensions as indeterminate fluids. *Science (Wash. DC).* 235:1511–1514.

Cassimeris, L., S. Inoue, and E. D. Salmon. 1988. Microtubule dynamics in the chromosomal spindle fiber. Analysis by fluorescence and high-resolution polarization microscopy. *Cell Motil. Cytoskeleton.* 10:185–196.

Craig, S.W., and T. D. Pollard. 1982. Actin binding proteins. *Trends Biochem. Sci.* 7:88–92.

Fechheimer, M., J. Brier, M. Rockwell, E. J. Luna, and D. L. Taylor. 1982. A calcium- and pH-regulated actin binding protein from *D. discoideum. Cell Motil.* 2:287–308.

Fisher, G. W., P. A. Conrad, R. L. Debiasio, and D. L. Taylor. 1988. Centripetal transport of cytoplasm, actin, and the cell surface in lamellipodia of fibroblasts. *Cell Motil.* 11:235–247.

Flory, P. J. 1953. Principles of polymer chemistry. Cornell University Press, Ithaca, NY. 342 pp.

Gershon, N. D., K. R. Porter, and B. L. Trus. 1985. The cytoplasmic matrix: its volume and surface area and the diffusion of molecules through it. *Proc. Natl. Acad. Sci. USA.* 82:5030–5034.

Hartwig, J. H., and T. P. Stossel. 1979. Cytochalasin B and the structure of actin gels. *J. Mol. Biol.* 134:539–553.

Hartwig, J. H., and T. P. Stossel. 1981. Structure of macrophage actin-binding protein molecules in solution and interaction with actin filaments. *J. Mol. Biol.* 145:563–581.

Heath, J. P. 1983. Behavior and structure of the leading lamella in moving

fibroblasts. I. Occurrence and centripetal movement of arc-shaped microfilament bundles beneath the dorsal cell surface. *J. Cell Sci.* 60:331–354.
Houk, T. W., and K. Ue. 1974. The measurement of actin concentration in solution: a comparison of methods. *Anal. Biochem.* 62:66–74.
Inman, J. K. 1975. Thymus-independent antigens: the preparation of covalent, hapten-Ficoll conjugates. *J. Immunol.* 114:704–709.
Inoue, S. 1981. Video image processing greatly enhances contrast, quality, and speed in polarization-based microscopy. *J. Cell Biol.* 89:346–356.
Jacobson, K. A., and J. W. Wojcieszyn. 1984. The translational mobility of substances within the cytoplasmic matrix. *Proc. Natl. Acad. Sci. USA.* 81:6747–6751.
Janmey, P. A., J. Peetermans, K. S. Zaner, T. P. Stossel, and T. Tanaka. 1986. Structure and mobility of actin filaments as measured by quasielastic light scattering, viscometry, and electron microscopy. *J. Biol. Chem.* 261:8357–8362.
Janmey, P. A., S. Hvidt, J. Peetermans, J. Lamb, J. D. Ferry, and T. P. Stossel. 1988. Viscoelasticity of F-actin and F-actin/gelsolin complexes. *Biochemistry.* 27:8218–8227.
Kane, R. E. 1975. Preparation and purification of polymerized actin from sea urchin egg extracts. *J. Cell Biol.* 66:305–315.
Kane, R. E. 1976. Actin polymerization and interaction with other proteins in temperature-induced gelation of sea urchin egg extracts. *J. Cell Biol.* 71: 704–714.
Kasai, M., S. A. Asakura, and F. Oosawa. 1962. The cooperative nature of G-F transformation of actin. *Biochim. Biophys. Acta.* 57:22–31.
Kathawalla, I. A., and J. L. Anderson. 1988. Pore size effects on diffusion of polystyrene in dilute solution. *Ind. Eng. Chem. Res.* 27:866–871.
Kawamura, M., and K. Maruyama. 1970. Electron microscopic particle length of F-actin polymerized in vitro. *J. Biochem.* 67:437–457.
Lanni, F., and B. R. Ware. 1984. Detection and characterization of actin monomers, oligomers, and filaments in solution by measurement of fluorescence photobleaching recovery. *Biophys. J.* 46:97–110.
Luby-Phelps, K. 1989. Preparation of fluorescently labeled Dextrans and Ficolls. *Methods Cell Biol.* 29:59–73.
Luby-Phelps, K., and D. L. Taylor. 1988. Subcellular compartmentalization by local differentiation of cytoplasmic structure. *Cell Motil.* 10:28–37.
Luby-Phelps, K., D. L. Taylor, and F. Lanni. 1986. Probing the structure of cytoplasm. *J. Cell Biol.* 102:2015–2022.
Luby-Phelps, K., P. E. Castle, D. L. Taylor, and F. Lanni. 1987. Hindered diffusion of inert tracer particles in the cytoplasm of mouse 3T3 cells. *Proc. Natl. Acad. Sci. USA.* 84:4910–4913.
Luby-Phelps, K., F. Lanni, and D. L. Taylor. 1988. The submicroscopic properties of cytoplasm as a determinant of cellular function. *Annu. Rev. Biophys. Biophys. Chem.* 17:369–396.
Mabuchi, I., and R. E. Kane. 1987. A 250 K-molecular-weight actin-binding protein from actin-based gels formed in sea urchin egg cytoplasmic extract. *J. Biochem.* 102:947–956.
MacLean-Fletcher, S. D., and T. D. Pollard. 1980. Viscometric analysis of the gelation of *Acanthamoeba* extracts and purification of two gelation factors. *J. Cell Biol.* 85:414–428.
Newman, J., N. Mroczka, and K. L. Schick. 1989. Dynamic light scattering measurements of the diffusion of probes in filamentous actin solutions. *Biopolymers.* 28:655–666.
Niederman, R., P. C. Amrein, and J. Hartwig. 1983. Three-dimensional structure of actin filaments and of an actin gel made with actin-binding protein. *J. Cell Biol.* 96:1400–1413.
Ogston, A. G. 1958. The spaces in a uniform suspension of fibres. *Trans. Faraday Soc.* 54:1754–1757.
Oosawa, F. 1970. Size distribution of protein polymers. *J. Theor. Biol.* 27:69–86.
Otto, J. J., R. E. Kane, and J. Bryan. 1979. Formation of filopodia in coelomocytes: localization of fascin, a 58,000 dalton actin cross-linking protein. *Cell.* 17:285–293.
Rockwell, M. A., M. Fechheimer, and D. L. Taylor. 1984. A comparison of methods used to characterize gelation of actin in vitro. *Cell Motil.* 4:197–213.
Rosenberg, S., A. Stracher, and R. C. Lucas. 1981. Isolation and characterization of actin and actin-binding protein from human platelets. *J. Cell Biol.* 91:201–211.
Schliwa, M., and J. van Blerkom. 1981. Structural interaction of cytoskeletal components. *J. Cell Biol.* 90:222–235.
Schnapp, B. J. 1986. Viewing single microtubules by video light microscopy. *Methods Enzymol.* 134:561–573.
Simon, J. R., R. H. Furukawa, B. R. Ware, and D. L. Taylor. 1988*a*. The molecular mobility of α-actinin and actin in a reconstituted model of gelation. *Cell Motil.* 11:64–82.
Simon, J. R., A. Gough, E. Urbanik, F. Wang, F. Lanni, B. R. Ware, and D. L. Taylor. 1988*b*. Analysis of rhodamine and fluorescein-labeled F-actin diffusion in vitro by fluorescence photobleaching recovery. *Biophys. J.* 54:801–815.
Spudich, J. A., and S. Watt. 1971. The regulation of rabbit skeletal muscle contraction. *J. Biol. Chem.* 246:4866–4871.
Stossel, T. P., J. H. Hartwig, H. L. Yin, K. S. Zaner, and O. I. Stendahl. 1981. Actin gelation and the structure of cortical cytoplasm. *Cold Spring Harbor Symp. Quant. Biol.* 46:569–578.
Tait, J. F., and C. Frieden. 1982. Polymerization and gelation of actin studied by fluorescence photobleaching recovery. *Biochemistry.* 21:3666–3674.
Tobacman, L. S., and E. D. Korn. 1983. The kinetics of actin nucleation and polymerization. *J. Biol. Chem.* 258:3207–3214.
Wang, K. 1977. Filamin, a new high-molecular-weight protein found in smooth muscle and nonmuscle cells: purification and properties of chicken gizzard filamin. *Biochemistry.* 16:1857–1865.
Wang, K., and S. J. Singer. 1977. Interaction of filamin with F-actin in solution. *Proc. Natl. Acad. Sci. USA.* 74:2021–2925.
Weihing, R. R. 1983. Purification of a HeLa cell high molecular weight actin binding protein and its identification in HeLa cell plasma membrane ghosts and intact HeLa cells. *Biochemistry.* 22:1839–1847.
Weihing, R. R. 1985. The filamins: properties and functions. *Can. J. Biochem. Cell Biol.* 63:397–413.
Wolosewick, J. J., and K. R. Porter. 1979. Microtrabecular lattice of the cytoplasmic ground substance. *J. Cell Biol.* 82:114–139.
Yguerabide, J., J. A. Schmidt, and E. E. Yguerabide. 1982. Lateral mobility in membranes as detected by fluorescence recovery after photobleaching. *Biophys. J.* 39:69–75.
Zaner, K. S., and T. P. Stossel. 1983. Physical basis of the rheologic properties of F-actin. *J. Biol. Chem.* 258:11004–11009.